12

NUMERICAL SIMULATIONS OF THE SEASONAL/LATITUDINAL VARIATIONS OF ATOMIC OXYGEN AND NITRIC OXIDE IN THE LOWER THERMOSPHERE AND MESOSPHERE

D. Rees and T. J. Fuller-Rowell

Department of Physics and Astronomy, University College London
Gower Street, London WC1E 6BT, United Kingdom

ABSTRACT:

A 2-Dimensional zonally-averaged thermospheric model and the global UCL thermospheric model have been used to investigate the seasonal, solar activity and geomagnetic variation of atomic oxygen and nitric oxide. The 2-Dimensional model includes detailed oxygen and nitrogen chemistry, with appropriate completion of the energy equation, by adding the thermal infrared cooling by [O] and [NO]. This solution includes solar and auroral production of odd nitrogen compounds and metastable species. This model has been used for three investigations: firstly, to study the interactions between atmospheric dynamics and minor species transport and density, secondly, to examine the seasonal variations of atomic oxygen and nitric oxide within the upper mesosphere and thermosphere and their response to solar and geomagnetic activity variations; thirdly, to study the factor of 7 - 8 peak nitric oxide density increase as solar $F_{10.7}$ cm flux increases from 70 to 240 reported from the Solar Mesospheric Explorer. Auroral production of [NO] is shown to be the dominant source at high latitudes, generating peak [NO] densities a factor of 10 greater than typical number densities at low latitudes. At low latitudes, the predicted variation of the peak [NO] density, near 110 km, with the solar $F_{10.7}$ cm flux is rather smaller than is observed. This is most likely due to an overestimate of the soft X-ray flux at low solar activity, for times of extremely low sunspot number, as occurred in June 1986. As observed on pressure levels, the variation of [O] density is small. The global circulation during solstice and periods of elevated geomagnetic activity causes depletion of [O] in regions of upwelling, and enhancements in regions of downwelling.

INTRODUCTION.

This paper provides a brief review of some two and three-dimensional model studies of the inter-relationships between the major and minor species of the lower thermosphere and upper mesosphere. Several timely questions are addressed by the model simulations. The data from the Solar Mesospheric Explorer (SME /1/) show a factor of about 7 - 8 variation of peak low-latitude number density as the solar $F_{10.7}$ cm flux increases from 70 to 240 units, compared with a variation of approximately a factor of 4 found in previous numerical studies /2/. The degree of possible variability of atomic oxygen number densities in the lower thermosphere and upper mesosphere consistent with major meteorological, seasonal and geomagnetic variability of the atmosphere is also of interest. Previous studies (for example a special issue of Planetary and Space Science, 1988) have shown up to a factor of at least 100 variability in the density of atomic oxygen at and below the peak density of the species, normally observed around 105 km.

ATOMIC OXYGEN AND NITRIC OXIDE: KEY MINOR CONSTITUENTS.

Atomic oxygen is created by the photodissociation of molecular oxygen within the thermosphere. Having approximately half the molecular mass of O_2 and N_2, its scale height is double that of O_2 and N_2 for the same temperature. Since recombination is very slow at middle and upper thermospheric densities and collision rates and if diffusive equilibrium prevails, [O] becomes the major constituent above around 150 km /3,4,5,6/. Given the long recombination time, the species can be transported globally by mean winds. When large-scale upwelling and advection occurs, particularly at solstice, and also associated with the intense large-scale heating during geomagnetic storms, diffusive equilibrium no longer fully controls the vertical profiles of [O] and [N_2, O_2]. Under such conditions /7,8/, the process known as wind-driven diffusion may cause large relative departures of individual light or heavy species from diffusive equilibrium, although hydrostatic equilibrium will

still be generally observed. Relative to density values which would be expected for the appropriate kinetic temperature, N_2 is strongly enhanced in regions of persistent upwelling and outflow, where atomic oxygen is strongly depleted. In regions of persistent convergence and downwelling, the converse is true. The major direct consequences are an excess of molecular nitrogen at the summer pole, particularly at times of high geomagnetic activity, while the winter pole (at quiet times) and winter mid-latitudes (under more disturbed conditions) contains the highest densities of atomic oxygen and helium.

These perturbations of minor species density extend to lower thermosphere altitudes, and wind-driven diffusion is one significant cause of variability of atomic oxygen in the lower thermosphere. Eddy diffusion can also cause vertical transport of minor species, and can change the vertical profile of atomic oxygen and other minor constituents /8/.

Nitric Oxide is primarily created through the reaction of the atomic nitrogen species $N(^2D)$ and $N(^4S)$ with molecular oxygen /3,9/. $N(^2D)$ and $N(^4S)$ are produced by auroral dissociation /10/, by photodissociation /11/ and various ion chemical reactions involving N_2^+ /12/.

Although nitric oxide is chemically and radiatively active, its chemical lifetime in the lower thermosphere is long enough for wind transport to be important. Its diffusion into the mesosphere is also important, and it has been shown /13/ that in the winter polar stratosphere, it also has a long effective lifetime in non-sunlit regions. Increased production, at times of high solar activity, or associated with enhanced auroral production during geomagnetic storms, may create very large lower thermospheric densities of [NO]. Given enhanced vertical transport due to turbulence, this may result in large [NO] densities in the mesosphere and even in the upper stratosphere at winter high-latitudes, where there is no solar photodestruction of nitric oxide. There are a number of major consequences of such enhancements, affecting the chemical and radiative balance of the mesosphere and thermosphere, and properties of the ionosphere.

THE NUMERICAL MODEL.

The three-dimensional atmospheric model has been well-described in a number of papers, including Fuller-Rowell and Rees /14,15/ and Fuller-Rowell et al /16/. The zonally-averaged model evolved from the nested grid model of Fuller-Rowell /17/ and is further described in Rees and Fuller-Rowell /8/.

The seasonal, latitudinal and solar activity variations of atomic oxygen density will be considered, as will the response to variable geomagnetic forcing at high geomagnetic latitude. Large-scale Hadley-type circulation cells are generated within the thermosphere, closing in the upper mesosphere, as the result of the solar diurnal heating variation, the seasonal / hemispheric asymmetry of solar heating, and due to geomagnetic heating, usually at high latitudes. These large-scale circulation systems force a partial breakdown of diffusive equilibrium as the result of the combination of vertical convection and horizontal advection. The full 3-dimensional global coupled ionosphere - thermosphere UCL model will be used for these simulations /14,15,16/.

A second series of simulations uses the zonally-averaged 2-dimensional model. Nitric oxide and other 'odd nitrogen' compounds are included as minor species. With this model, it is possible to examine, in addition, the seasonal, latitudinal, solar activity and geomagnetic response of [NO]. It is also possible to evaluate the transport and thermal effects of variable eddy turbulence within the lower thermosphere and upper mesosphere. The model takes into account the thermal radiation from nitric oxide, which has very important effects on the thermal balance, and consequences for the mean circulation.

The two-dimensional, zonally-averaged model of the thermosphere solves the non-linear energy, momentum, continuity and three-constituent composition equation self-consistently and time-dependently. The finite-difference grid covers the latitude range from the north to the south geographic pole in steps of 5° latitude, and the seventeen pressure levels, one scale height apart, cover altitudes from 70km to approximately 500km, depending on solar activity. The model has been adapted from the high-resolution, nested-grid model of Fuller-Rowell /17/, which contains a complete description of the numerical procedure, the set of equations, boundary conditions and parameterisation required to simulate the thermospheric neutral wind, temperature and density. The same paper also describes the photochemistry, and the dissociation and recombination rate constants included in the computation of the mass mixing ratio of the major species of atomic oxygen, and of molecular nitrogen and oxygen.

A further addition has been made to the model to include the production, loss and transport of $N(^2D)$, $N(^4S)$, and NO (Nitric Oxide). The evolution of the concentrations of these minor species are computed self-consistently in parallel with the development of the structure, dynamics and energy budget of the major species. The creation of nitric oxide occurs through the odd-nitrogen chemistry primarily through the reactions of $N(^2D)$ and $N(4^S)$ with molecular

oxygen. The $N(^2D)$ and $N(^4S)$ are produced by ion chemical reactions involving N_2^+, and by direct dissociation of N_2 by auroral particles /10/ or solar radiation /11/. The odd-nitrogen chemistry, branching ratios, and rate coefficients, included in the model are as described in Roble et al /2/.

All three production sources of atomic nitrogen are included in the zonally averaged model. The sources of $N(^2D)$ and $N(^4S)$ through the ion chemical reactions are evaluated within the UCL-Sheffield coupled thermosphere-ionosphere model. The reference spectra appropriate for high and low solar activity, together with the ionisation frequencies of the major species, are taken from Torr et al /18/. The solar production function thus produced is used within the zonally averaged code, where solution of the odd nitrogen chemistry and transport proceeds in parallel with that of the dynamics, energy budget and composition of the major species.

The particle precipitation source is derived from the TIROS/NOAA satellite data /19/ and is used to describe the high-latitude auroral heating rate, ionization rate, and molecular nitrogen dissociation /10/, self-consistently within the model. The direct particle heating acts in addition to the Joule dissipation which together modify the global circulation pattern. The circulation, which transports and mixes the major species and is described fully in Fuller-Rowell /17/, also acts as a source of transport to the minor species. The distribution of nitric oxide, as a strong radiative cooler /9/, has a strong influence on the latitudinal temperature gradient, and on the global mean thermospheric temperature as has been shown by Roble and Emery /20/. The latitudinal distribution of temperature and NO, and the global circulation pattern, is a highly coupled and interacting system of variables.

The auroral precipitation also produces ionization which enhances the ion densities above the quiet background levels described by Chiu /21/. This additional source of ionization has been included, where the auroral enhancement is assumed to be in chemical equilibrium, and is added to the background solar-produced values of Chiu /21/ by the square root of the sum of the squares. This is a less sophisticated approach than is used in the 3-D fully-coupled ionosphere - thermosphere model, but produces an overall result which is adequate for the purposes of these 2-D simulations, where we are not yet concerned with the details of the ionospheric predictions.

RESULTS OF THE SIMULATIONS.

Global distributions with seasonal, latitudinal and geomagnetic variations.

Figure 1 shows the global distributions of temperature, mean molecular mass, atomic oxygen density and molecular nitrogen density at pressure level 7 (125 km) of the UCL three-dimensional, time-dependent model (E-Region, approximately 125 km). The seasonal / latitudinal variation of atomic oxygen density shows a very distinct minimum at the summer pole, and a maximum at the winter pole. For moderately active solar ($F_{10.7}$ - 185), and quiet geomagnetic activity conditions, there is a factor of more than 2 variation of E-region atomic oxygen density from global minimum to global maximum. This simulation includes the effect of lower atmosphere tides introduced via lower boundary forcing /22/.

Figure 2 shows the global distributions of temperature, mean molecular mass, atomic oxygen density and molecular nitrogen density at pressure level 12 of the UCL three-dimensional, time-dependent model (F-Region, approximately 320 km). There is a very large seasonal / latitudinal variation of atomic oxygen density. The minimum oxygen density is at the summer pole, however, the maximum values are displaced from the winter pole, towards high winter mid-latitudes, as a result of high-latitude energy input. This simulation is for moderately active solar ($F_{10.7}$ - 185), and moderately disturbed geomagnetic activity conditions (Kp - 3). Atomic oxygen number density varies by more than a factor of 6 from global minimum to global maximum, consistent with empirical model results /16/.

Figure 3 shows the global distributions of temperature, mean molecular mass, atomic oxygen density and molecular nitrogen density at pressure level 7 of the UCL three-dimensional, time-dependent model (E-Region, approximately 125 km) taken from the same simulation as that shown in Figure 2. It shows that a similar, if somewhat smaller seasonal / latitudinal variation of atomic oxygen density occurs at the lower altitudes. The minimum oxygen density is again at the summer pole and, as at F-region altitudes, the maximum values are displaced from the winter pole, towards high winter mid-latitudes, as a result of high-latitude energy input. There is a surprisingly large variation of atomic oxygen density from global minimum to global maximum, about a factor of 5, resulting from the seasonal asymmetry of solar insolation, combined with the high-latitude geomagnetic energy input. This factor of 5 atomic oxygen density variation at ~125 km altitude greatly exceeds the latitudinal / seasonal total density variation. It is necessary to recall that the majority of species density profiles are measured with sole reference to geometric altitude, and no reference to pressure level or to total gas density.
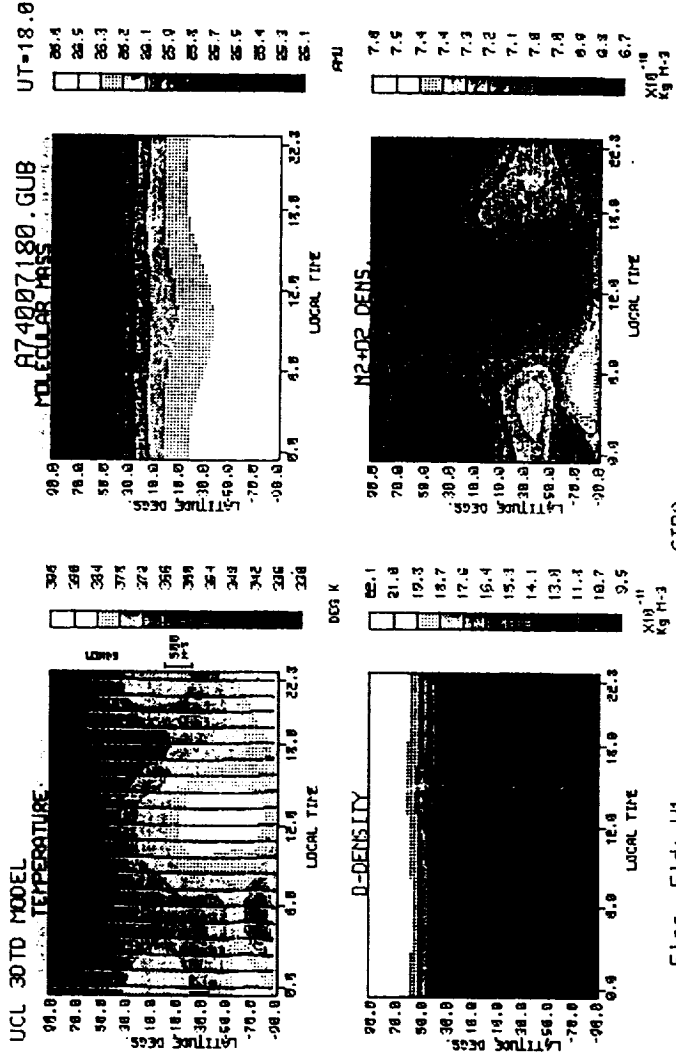
FIGURE 1. Pressure level 7 of the UCL three-dimensional, time-dependent model (E-REGION, approximately 125 km) for moderately active solar conditions ($F_{10.7} = 185$) and quiet geomagnetic activity conditions. There is a factor of more than 2 variation of E-region atomic oxygen density from global minimum to global maximum.
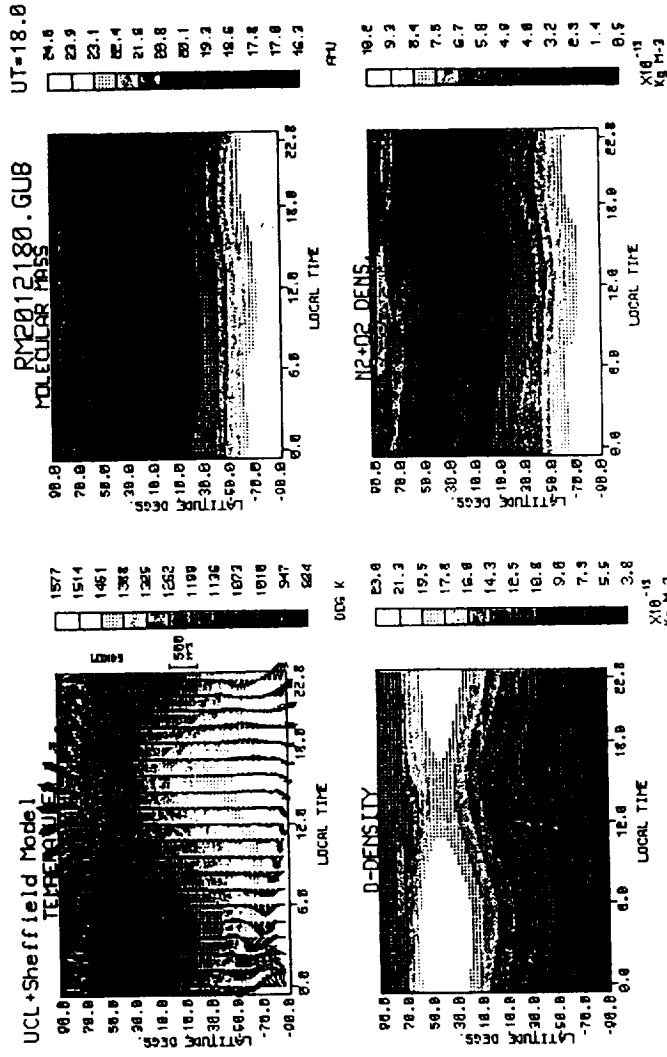
FIGURE 2. Pressure level 12 of the UCL three-dimensional, time-dependent model (F-REGION, approximately 320 km) from a simulation for moderately disturbed geomagnetic activity conditions, and for moderately active solar conditions ($F_{10.7} = 185$). The minimum oxygen density is at the summer pole, but the maximum values are displaced from the winter pole, towards high winter mid-latitudes.
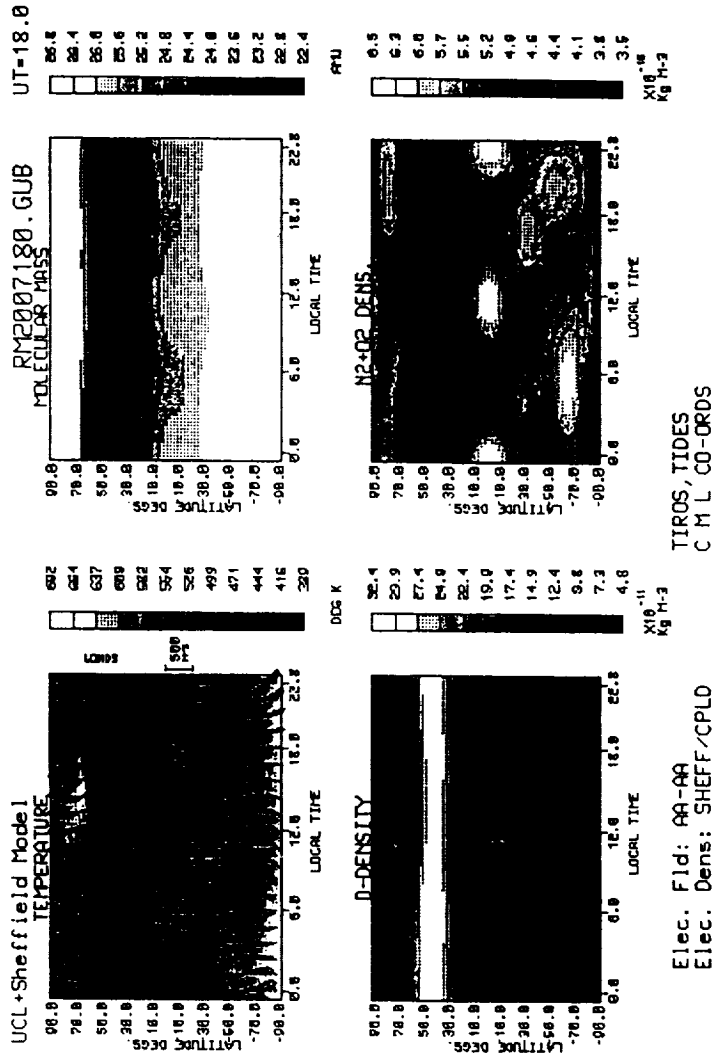
FIGURE 3. Pressure level 7 of the UCL three-dimensional, time-dependent model (E-REGION, approximately 125 km) for the same simulation as that shown in Figure 2. The minimum oxygen density is again at the summer pole and, as at F-region altitudes, however, the maximum values are displaced from the winter pole, towards high winter mid-latitudes.

Latitudinal distributions for equinox and variations with solar and geomagnetic activity.

Figure 4 shows variations of atmospheric structure and composition as a function of altitude and latitude simulated using the two-dimensional, time-dependent model. Panel A shows the density distributions of atomic oxygen, nitric oxide, molecular oxygen and molecular nitrogen. Panel B shows Temperature, Meridional and vertical neutral wind, and mean molecular mass. Panel C displays nitric oxide density distribution from 100 to 160 km, for comparison with the results obtained from SME /1/. The conditions depicted are equinox, low solar ($F_{10.7}$ cm - 80) and low geomagnetic (Kp - 1) activity. There is a weak latitudinal variation of atomic oxygen density, caused by the high-latitude geomagnetic energy inputs. Nitric oxide density is structured by two peaks, one at low-latitudes, due to solar production, and the other in the auroral oval, resulting from auroral particle dissociation.

Figure 5 shows variations of atmospheric structure and composition as a function of altitude and latitude simulated using the two-dimensional, time-dependent model. The displays are as for Figure 4. The conditions simulated are low solar ($F_{10.7}$ cm - 80) and moderate geomagnetic activity (Kp - 3), at equinox. There is now a small latitudinal variation of atomic oxygen density, with decreased density in regions of increased high-latitude geomagnetic energy inputs. The major feature in nitric oxide density is the enhanced high-latitude peaks, resulting from increased auroral production. There is a ratio of about 4:1 between low-latitude and high latitude values of nitric oxide.

Figure 6 shows variations of atmospheric structure and composition as a function of altitude and latitude simulated using the two-dimensional, time-dependent model. The displays are as for Figure 4. The conditions which are simulated are low solar ($F_{10.7}$ cm - 80) and high geomagnetic activity (Kp -5), at equinox. The latitudinal variation is further enhanced. Atomic oxygen is further depleted, and molecular nitrogen further enhanced, in those regions which correspond to the enhanced auroral energy and particle inputs. Nitric oxide densities vary by an order of magnitude from low to high latitudes. The broad latitude extension of elevated nitric oxide densities correspond mainly to the extended regions of energetic particle precipitation described by the statistical models of energetic electron precipitation. Marked changes of nitric oxide extend to the lower altitude limits (70 km) of the model, while significant changes of atomic oxygen density extend below 86 km. These low-altitude disturbances are primarily due to intense geomagnetic energy inputs within the auroral oval.

Figure 7 shows variations of atmospheric structure and composition as a function of altitude and latitude simulated using the two-dimensional, time-dependent model. The displays are as for Figure 4. The conditions which are simulated are high solar activity ($F_{10.7}$ cm - 200), and low geomagnetic activity (Kp - 2) at equinox. There are considerable enhancements of molecular nitrogen, molecular oxygen and nitric oxide densities and a marked decrease of atomic oxygen density within both auroral ovals. At this high level of solar activity, the low latitude values of nitric oxide density are considerably increased, by about a factor of 4, compared with those for low solar activity ($F_{10.7}$ cm - 80). This factor is smaller than the factor of 7 - 8 reported for the same range of solar activity by Barth /1/. This apparent discrepancy will be discussed in the following section. Even at high solar activity, the low latitude values remain below the peak auroral oval values, except for very quiet geomagnetic conditions, Kp - 1 or lower. This indicates that except for prolonged periods of geomagnetic quiet during periods of high solar radio and UV / EUV fluxes, high latitude peaks, corresponding to enhanced auroral production, will still be a distinctive feature of the global distribution of nitric oxide.

Latitudinal distributions for solstice.

Figure 8 shows variations of atmospheric structure and composition as a function of altitude and latitude simulated using the two-dimensional, time-dependent model. The displays are as for Figure 4. The conditions which are simulated are moderately high solar activity ($F_{10.7}$ cm - 150), and low geomagnetic activity (Kp - 2) at the December solstice. A significant seasonal / latitudinal asymmetry develops in the distribution of all constituents. There is a large summer high latitude enhancement of molecular nitrogen and of nitric oxide, and depletion of atomic oxygen. For nitric oxide, there is approximately a factor of 50 % summer high latitude enhancement, the combination of solar and auroral production. For atomic oxygen and molecular nitrogen, the behaviour in the summer and winter hemispheres is quite opposite, due to the influence of global, pole to pole circulation. For nitric oxide, there is still an enhancement in the winter auroral oval, as well as the rather larger enhancement in the summer auroral oval.

DISCUSSION.

Atomic oxygen in the upper thermosphere shows large seasonal / latitudinal variations in response to asymmetric solar insolation. Such variations have been well known for many years, and have now been successfully simulated by theoretical and numerical modelling.

LOG10(NO) CM−3   LOG10(O) CM−3
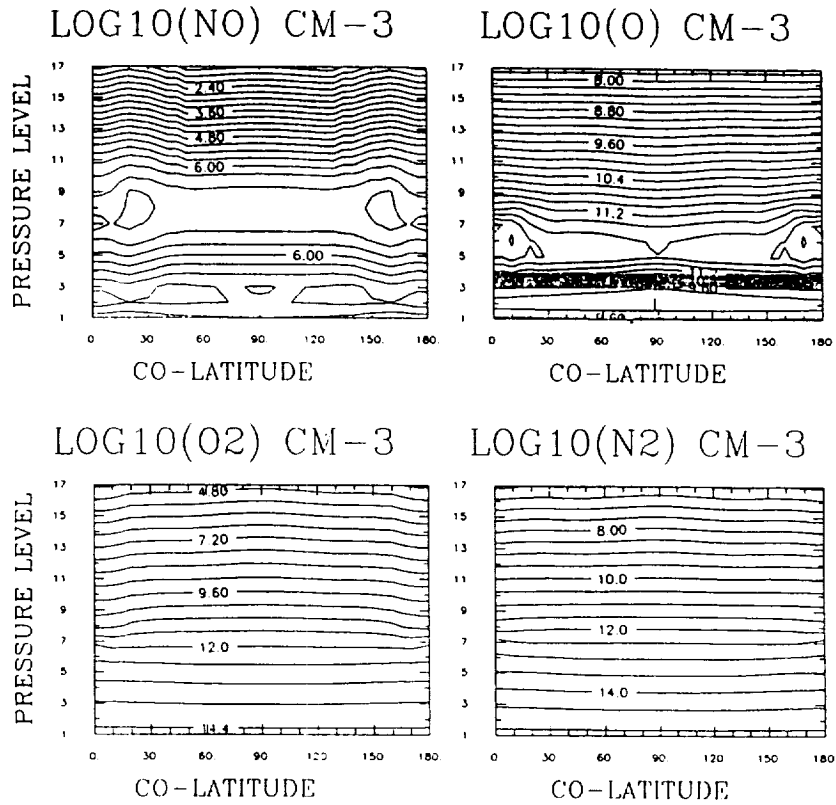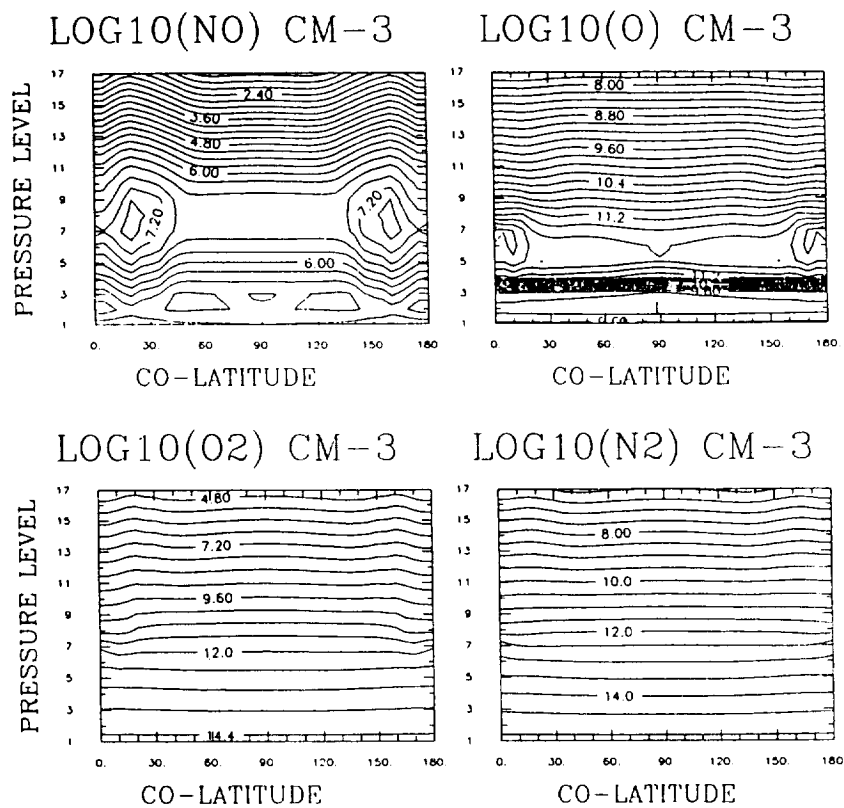
LOG10(O2) CM−3   LOG10(N2) CM−3

Figure 4. Variations of atmospheric structure and composition as a function of altitude and latitude, simulated using the UCL two-dimensional, time-dependent model. Panel A shows the density distributions of atomic oxygen, nitric oxide, molecular oxygen and molecular nitrogen. Panel B shows temperature, meridional and vertical neutral wind, and mean molecular mass. The conditions depicted are equinox, low solar ($F_{10.7}$ cm = 80) and low geomagnetic activity (Kp = 1). Panel C depicts the distribution of nitric oxide between 100 and 160 km, for direct comparison with the data from SME.
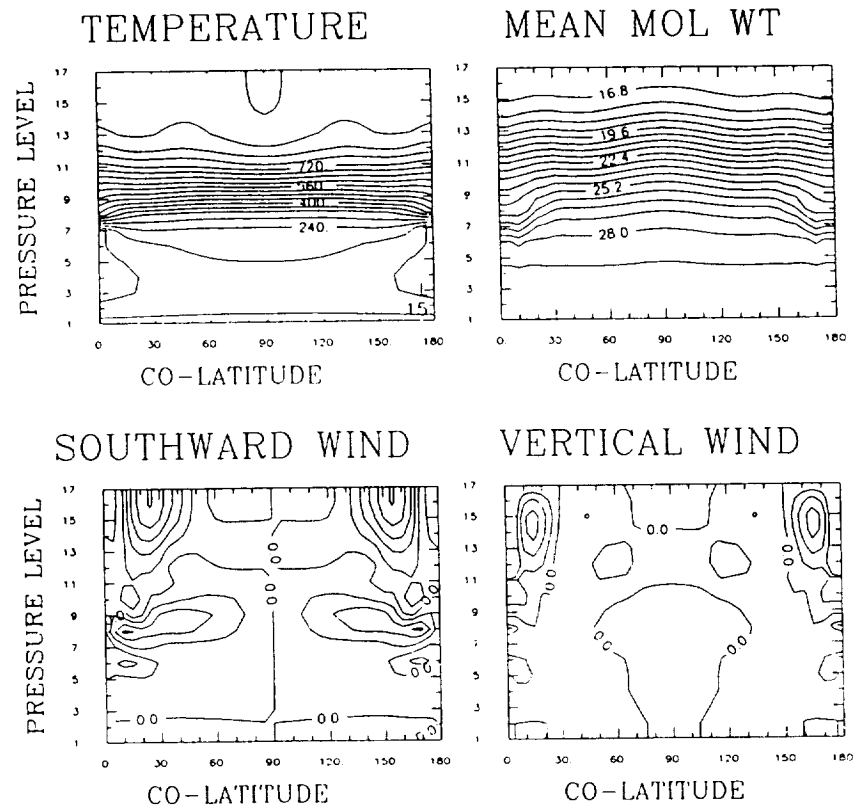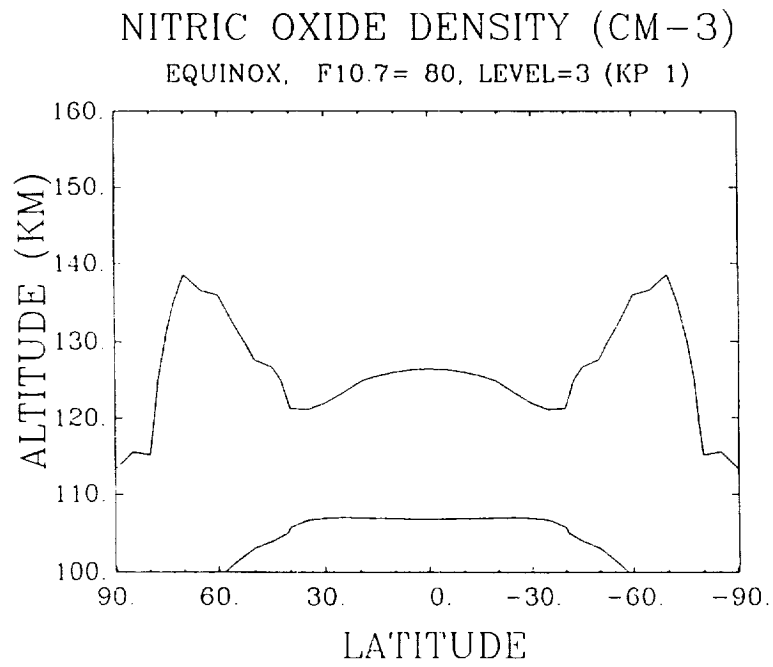
TEMPERATURE

MEAN MOL WT

SOUTHWARD WIND

VERTICAL WIND

Figure 4B.

NITRIC OXIDE DENSITY (CM−3)
EQUINOX, F10.7= 80, LEVEL=3 (KP 1)

CONTOUR FROM 0.50000E+07 TO 0.60000E+08 CONTOUR INTERVA OF 0.5000E+07PT(3,3)= 0.56344E+0.LABELS SCALED BY 0.10000E-04

Figure 4C.

LOG10(NO) CM-3   LOG10(O) CM-3

LOG10(O2) CM-3   LOG10(N2) CM-3

Figure 5. Variations of atmospheric structure and composition as a function of altitude and latitude simulated using the two-dimensional, time-dependent model. The display is as for Figure 4. The conditions simulated are low solar ($F_{10.7}$ cm = 80) and moderate geomagnetic activity (Kp = 3) at equinox.
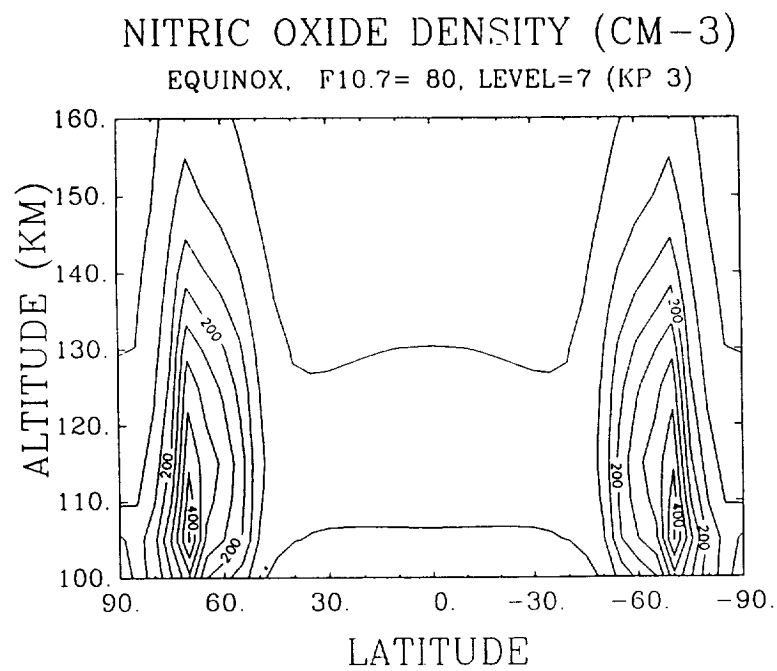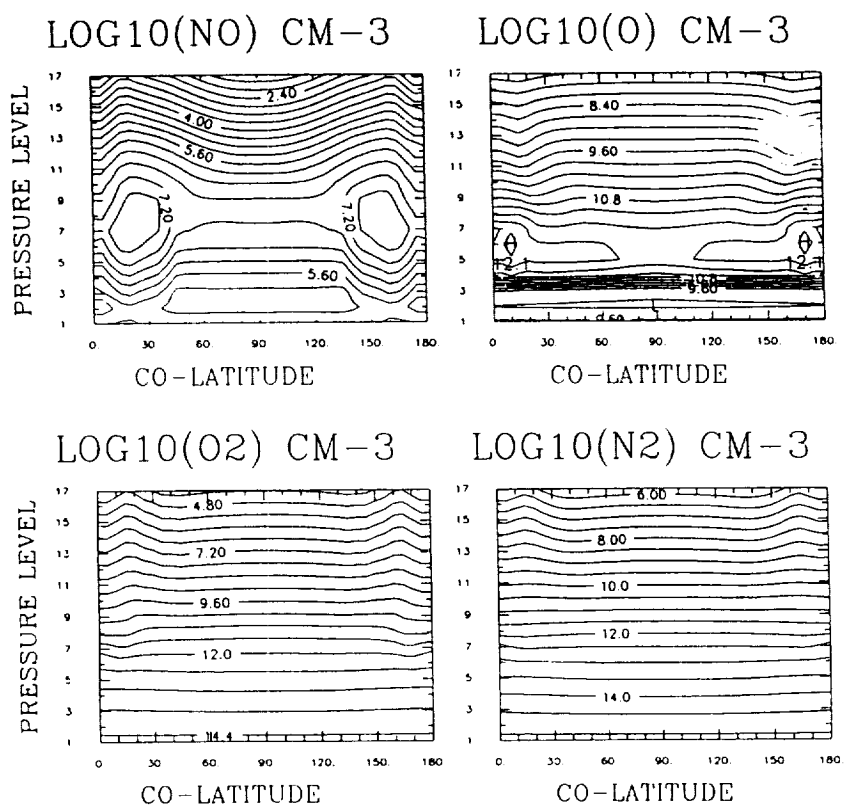
Figure 5B.

NITRIC OXIDE DENSITY (CM−3)

EQUINOX, F10.7= 80, LEVEL=7 (KP 3)

CONTOUR FROM 0 50000E+07 TO 0 60000E+08 CONTOUR INTERVA OF 0 50000E+07 (L 3) 0 1472.1 FON ANELS SCALED BY 0 10000E-04

Figure 5C.

LOG10(NO) CM-3   LOG10(O) CM-3

LOG10(O2) CM-3   LOG10(N2) CM-3

Figure 6. Variations of atmospheric structure and composition as a function of altitude and latitude simulated using the two-dimensional, time-dependent model. The display is as for Figure 4. The conditions which are simulated are low solar ($F_{10.7}$ cm = 80) and moderately high geomagnetic activity (Kp = 5) at equinox.

TEMPERATURE
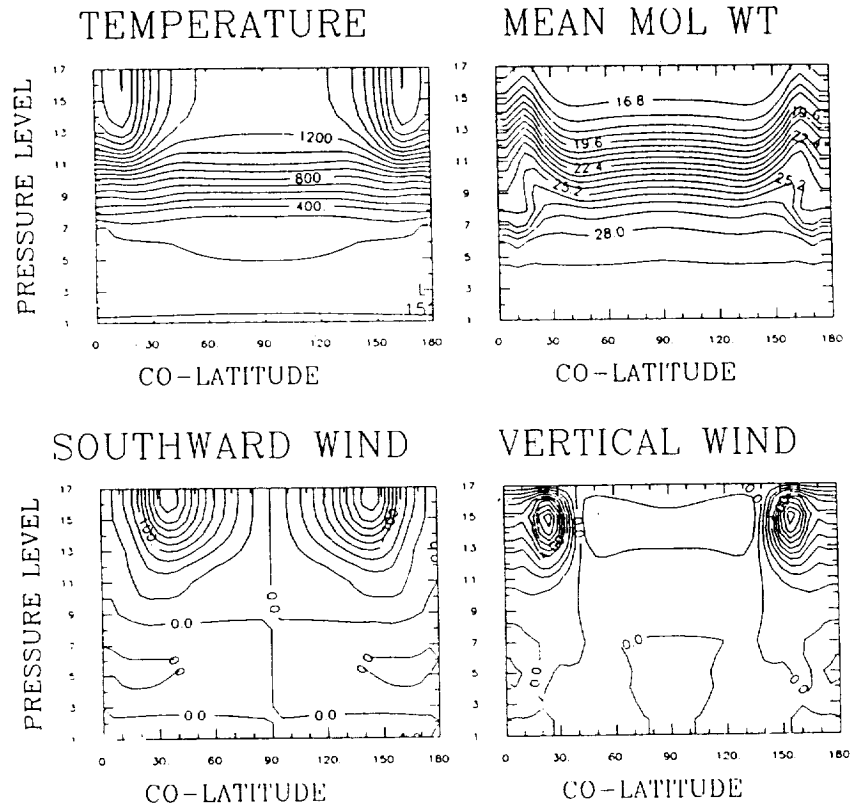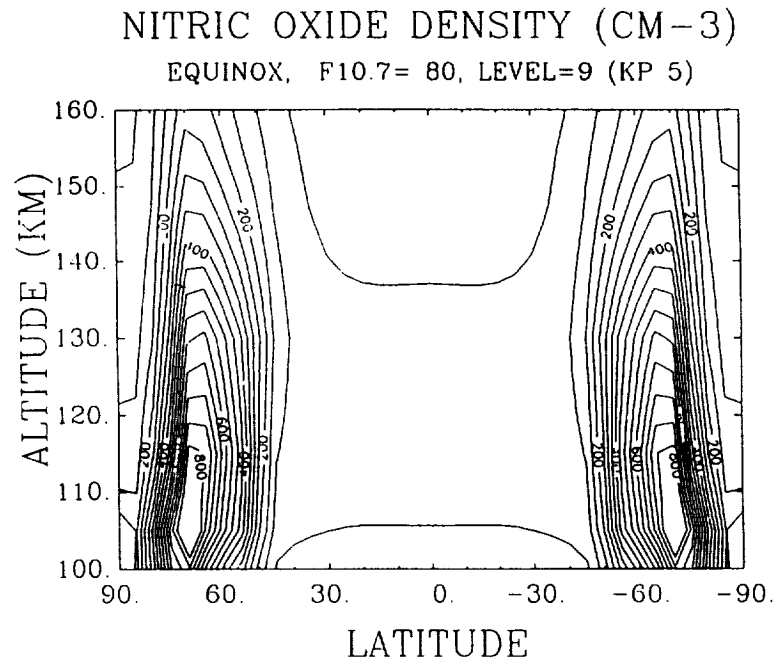

MEAN MOL WT

SOUTHWARD WIND

VERTICAL WIND

Figure 6B.

NITRIC OXIDE DENSITY (CM−3)

EQUINOX, F10.7= 80, LEVEL=9 (KP 5)

Figure 6C.

LOG10(NO) CM-3   LOG10(O) CM-3
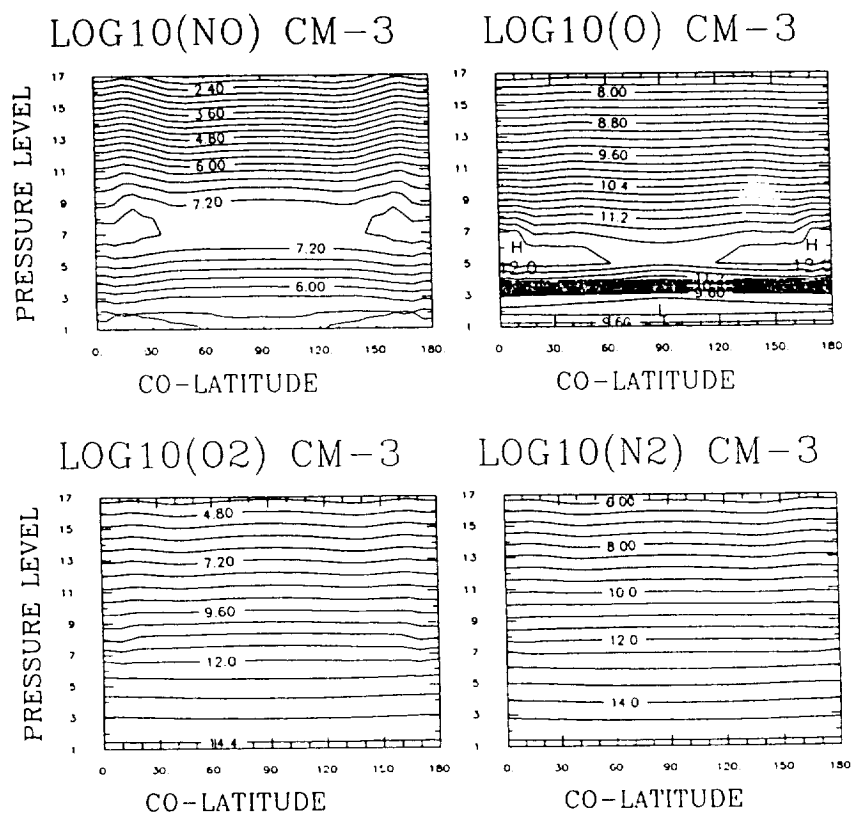
LOG10(O2) CM-3   LOG10(N2) CM-3

Figure 7. Variations of atmospheric structure and composition as a function of altitude and latitude simulated using the two-dimensional, time-dependent model. the display is as for Figure 4. The conditions which are simulated are high solar ($F_{10.7}$ cm = 200) and low geomagnetic activity (Kp = 2) at equinox.

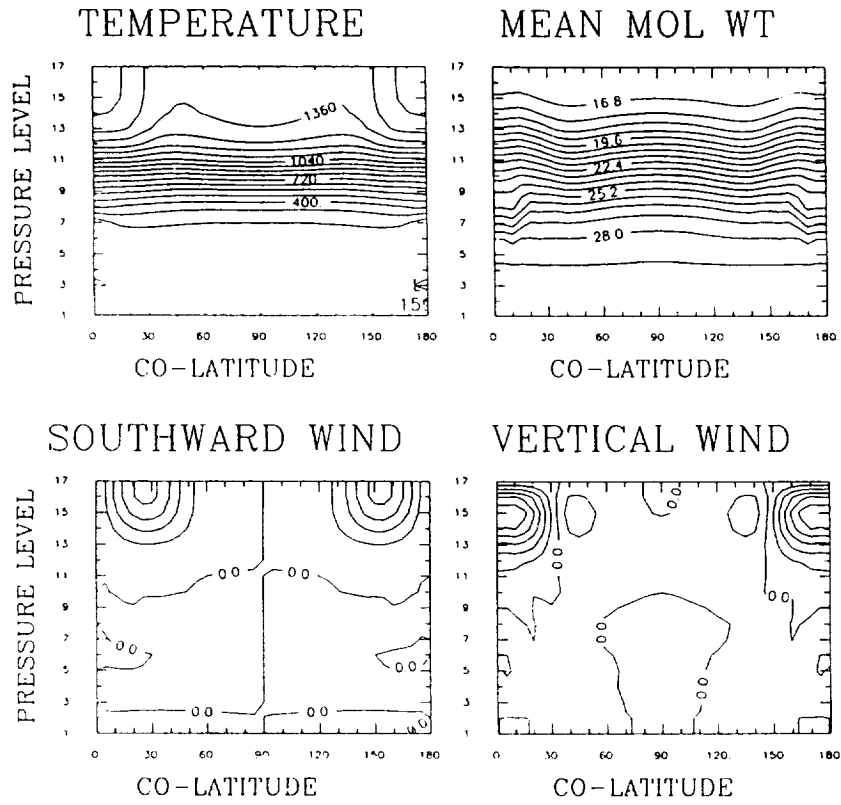TEMPERATURE — MEAN MOL WT — SOUTHWARD WIND — VERTICAL WIND

Figure 7B.

NITRIC OXIDE DENSITY (CM−3)
EQUINOX, F10.7=200, LEVEL=5 (KP 2)

CONTOUR FROM 0.50000E+07 TO 0.80000E+08 CONTOUR INTERVAL OF 0.50000E+07P1(3.3)= 0.34411E+08LABELS SCALED BY 0.10000E−04

Figure 7C.

174
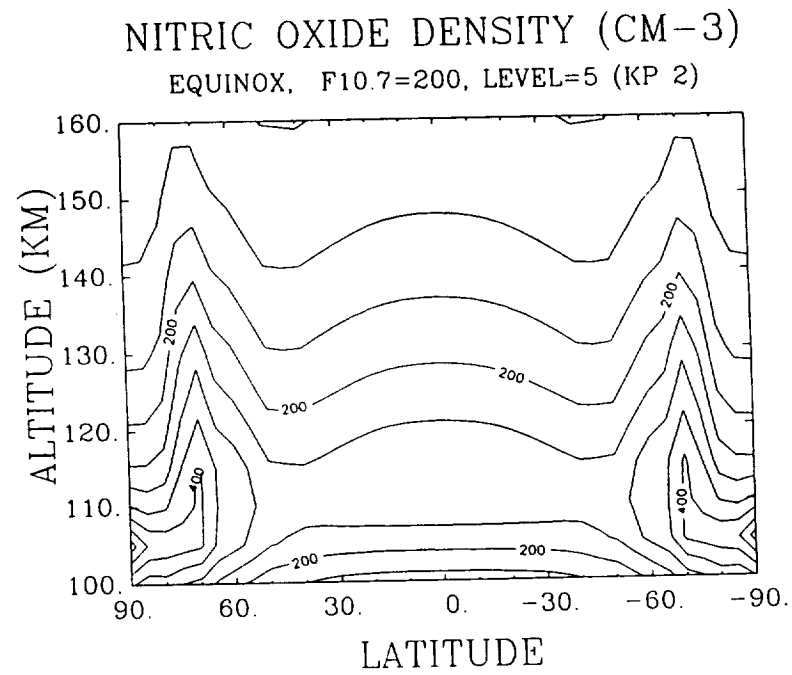
LOG10(NO) CM−3   LOG10(O) CM−3
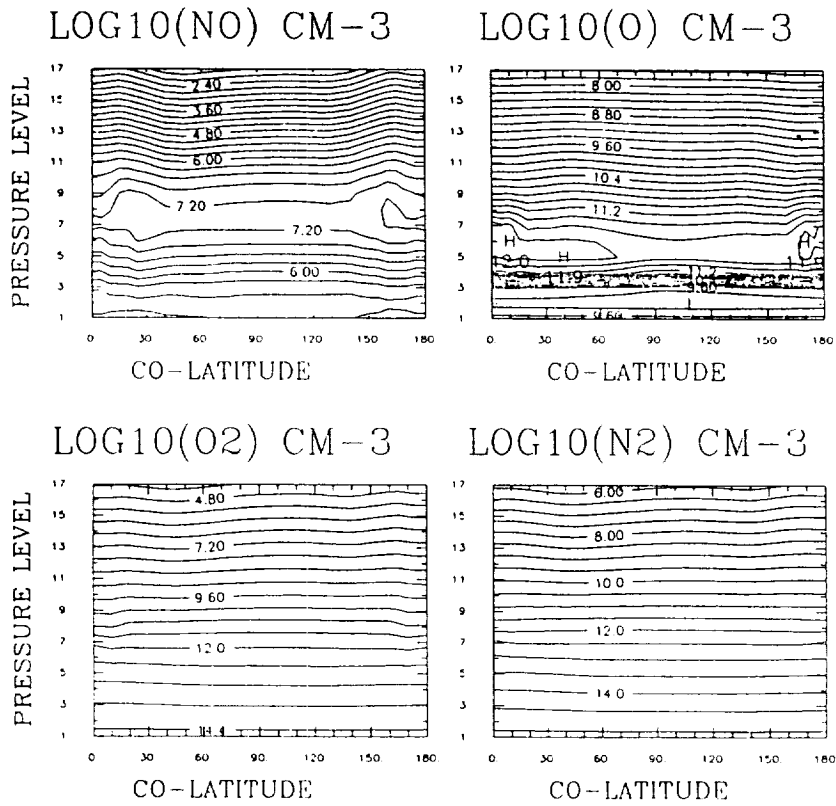
LOG10(O2) CM−3   LOG10(N2) CM−3

Figure 8. Variations of atmospheric structure and composition as a function of altitude and latitude simulated using the two-dimensional, time-dependent model. The display is as for Figure 4. The conditions depicted are moderately high solar activity ($F_{10.7}$ cm = 150) and low geomagnetic activity (Kp = 2) at the December solstice.

TEMPERATURE
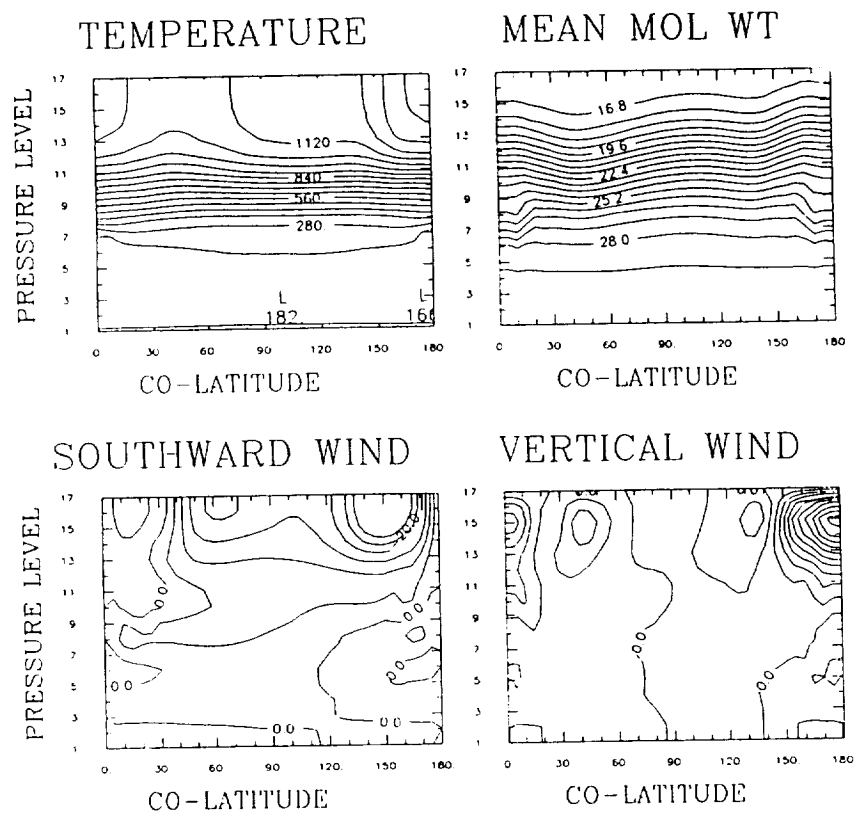

MEAN MOL WT

SOUTHWARD WIND

VERTICAL WIND

Figure 8B.

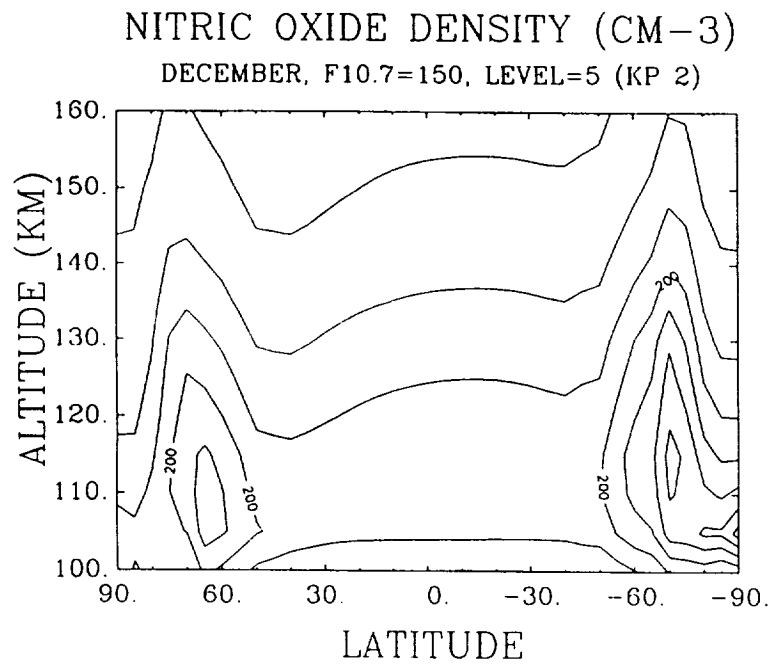# NITRIC OXIDE DENSITY (CM−3)

DECEMBER, F10.7=150, LEVEL=5 (KP 2)

CONTOUR FROM 0 50000E+07 TO 0 60000E+08 CONTOUR INTERVAL OF   0 50000E+07PI(3,3)= 0 1615BE+08LABELS SCALED BY   0 10000E-04

Figure 8C.

Wind-driven diffusion /23/ caused by systematic upwelling over the summer pole, downwelling near the winter pole, with an interconnecting mean meridional flow of the order of 50 m/sec, partly overcomes diffusive equilibrium within the thermosphere. This causes the enhancement of heavy atomic and molecular species relative to light atomic species in the summer polar region and the converse in the region of downwelling near the winter pole.

At higher levels of geomagnetic activity, the wind-driven diffusion process is enhanced, causing a further enrichment of heavy and molecular species in the summer geomagnetic polar cap, where the strongest combined solar and geomagnetic heating occurs. At such times, the latitudinal variations of the atomic oxygen mixing ratio in the upper thermosphere become both larger and more complex, particularly at the solstice. Using coupled ionosphere - thermosphere models, the structures observed during major disturbances can be reasonably well simulated, and related to the locally-enhanced heating and upwelling caused, in the polar regions, by enhanced ion-neutral coupling (ion drag / frictional / Joule heating) resulting from the enhancement of E-region plasma densities by particle precipitation.

Under disturbed geomagnetic conditions at solstice, there can be a factor of 10 latitude variation in atomic oxygen concentration at the same F-region altitude (300 km). Even at E-region altitudes (around 125 km), a factor of 5 variation can occur. In both cases, minimum [O] values are within the summer geomagnetic polar cap, while maximum [O] values are at high winter mid-latitudes, equatorward of the auroral oval.

It is clear from the figures that the dominant influence on global [NO] production is from the auroral dissociation of N_2 at high latitudes. For all but the most quiet geomagnetic conditions, the high latitude peak NO number density is considerably greater than values observed at equatorial latitudes. At low latitudes, however, a large variation over the solar cycle has been observed /1/. This is a direct result of the solar cycle-related flux increase in the wavelength range up to 100 nm.

The solar production of $N(^2D)$ and (N^4S), the precursors of [NO], occurs primarily through the ion chemical reactions, particularly N_2^+ with neutral oxygen. A small additional source has also been identified by Richards et al /11/, namely the predissociation of N_2 in the wavelength range 80 - 100 nm. The peak [NO] density, near 105 km, is strongly controlled at low latitudes by the strength of the solar ionising flux able to penetrate to these levels. The wavelength region of most interest therefore, is the 1 - 14 nm soft X-ray flux.

The present simulations have used the solar fluxes and ionisation frequencies of the major species described by Torr et al /18/. The reference spectrum for low solar activity is from rocket-borne measurements in April 1974, when the $F_{10.7}$ cm radio flux was about 70 units. For high solar activity, the period in June 1979 was used, when the $F_{10.7}$ cm flux was in excess of 240 units. Using these reference spectra to define the range of solar flux in the model, the peak low-latitude [NO] density around 110 km varied from 0.8 * 106 cm-3 at low solar activity, to 3 * 106 cm-3 at high solar activity. The [NO] values differ from the observations of Barth /1/ over the last solar cycle. He reported a variation of a factor of 7 - 8 for the ratio of peak equatorial [NO] from high to low solar activity. The only fundamental difference with the present results is that the model appears to underestimate the minimum values by a factor of 2, and hence underestimates the ratio of equatorial [NO] density from high to low solar activity.

The most plausible explanation is that the soft X-ray flux was actually lower during the last solar cycle minimum in June 1986, than in the April 1974 minimum period, when direct solar EUV radiance measurements were available. Although the $F_{10.7}$ cm radio flux was similar during the two periods, the sunspot numbers differed considerably. In April 1974, the sunspot number was 40, in 1986, the minimum value was 1 during June, and the 1986 average only 14. In view of the strong correlation of the E-region critical frequency with the Zurich sunspot number, a direct relationship between [NO] density and the soft X-ray flux appears the most likely explanation. The $F_{10.7}$ cm radio index is thus not a particularly good indicator of [NO] equatorial density, and an index related to sunspot number might provide a better key for prediction.

We have previously shown /8/ that increased eddy turbulence causes enhanced downward transport of nitric oxide from the upper thermosphere to the mesosphere. The number density of nitric oxide is increased in the lower thermosphere, at the mesopause, and in the upper mesosphere by more than a factor of 10 by enhanced values of eddy turbulence (within published values).

The dominant consequence of the enhanced downward transport of nitric oxide is strong mesopause cooling in the vicinity of the region of enhanced eddy diffusion coefficient. The cooling is due to increased I.R. radiation from regions of elevated nitric oxide density. There is a change in the mean meridional wind and flow towards regions of increased eddy turbulence, which causes a complex sequence of inter-related effects.

If eddy turbulence is increased systematically on a large scale, for a period of several days, mesospheric nitric oxide densities increase. This causes, via increased radiative cooling, mesopause cooling of the order of 30 K, in the region of enhanced eddy turbulence. The increased eddy transport also enhances upper mesospheric atomic oxygen densities, but less dramatically than for nitric oxide, since atomic oxygen is removed rather rapidly below about 95 to 100 km.

SUMMARY.

In this study, we have attempted to use the numerical models to study the range of variability of atomic oxygen and nitric oxide which might be expected to occur as the result of four fundamental processes of change affecting the lower and upper thermosphere.

(1) Seasonal / latitudinal variations.

The effect of global convection and advection induced by asymmetric solar isolation near solstice causes a strong latitudinal variation in the composition of the thermosphere. Systematic upwelling and outflow near the summer pole, the connecting circulation and systematic convergence and downwelling towards the winter pole disturb diffusive equilibrium. The result is the enhancement of heavy atomic and molecular species, as viewed at constant pressure levels, in the summer polar regions, and a complementary enhancement of light atomic species near the winter polar region (again relative to constant pressure levels). The effects are well-determined empirically, and the seasonal / latitudinal variation is further enhanced by the high latitude heating during periods of high geomagnetic activity.

In the summer polar region, the mean molecular mass at pressure level 12 (F-region, around 300 km) may increase to above 24 / 25 amu (high solar activity, $F_{10.7} - 185$, and for moderately disturbed geomagnetic conditions, Kp $- 3^+ - 5$). The minimum mean molecular mass at pressure level 12 (around 280 km) is now at high winter mid-latitudes (rather than in the winter polar region) but still has a value close to 17 amu.

Such compositional disturbances are not confined to the F-region, and even at 125 km, variations of a factor of 5 in atomic oxygen density can be generated at high geomagnetic activity levels.

For nitric oxide, there is approximately a 50 % modulation in number density caused by seasonal variations.

Solar Activity variations.

The latitude variations observed at constant pressure levels in atomic oxygen and molecular nitrogen caused by seasonal asymmetries of illumination and heating are only marginally changed by variations of solar activity. However, nitric oxide responds quite dramatically. The simulated variation of a factor of 4, as solar $F_{10.7}$ cm flux increases from 70 to 240, is smaller than the ratio reported from SME observations - a factor of 7 - 8. This difference is most likely associated with smaller X-ray fluxes during the 1986 solar minimum than during 1074, the previous solar cycle minimum. During 1986, the sunspot number was exceptionally low.

Geomagnetic Activity Variations.

The relatively localised energy inputs associated with elevated levels of geomagnetic activity generally decrease atomic oxygen concentrations (when observed on constant pressure levels). In the summer polar cap, this decrease can be an order of magnitude at F-region altitudes (around 300 km), and a factor of 5 at E-region altitudes (125 km). Normally, molecular nitrogen densities are elevated as the atomic oxygen density decreases. Nitric oxide generally responds quickly and increases rapidly in response to an increase of auroral production, varying by more than one order of magnitude from quiet to disturbed geomagnetic conditions.

Effects of eddy turbulence transport:

Atomic Oxygen.

Increased eddy turbulence causes enhanced downward transport of atomic oxygen from the upper thermosphere into the mesosphere. Where eddy turbulence is enhanced, the mixing ratio of [O] is increased at all altitudes, not only in the vicinity of the mesopause and lower thermosphere.

Nitric Oxide.

Nitric Oxide is readily transported downward by enhanced eddy diffusion around and above the mesopause. This may enhance radiative cooling of the upper mesosphere caused by nitric oxide, with further signatures in temperature and wind distributions.

A combination of seasonal, solar activity and geomagnetic variations discussed in this paper can cause unusual values or profiles of nitric oxide or atomic oxygen within the lower thermosphere and upper mesosphere. Generally, there should be a correlation or anticorrelation between variations of different major and minor constituents, within the lower thermosphere and upper mesosphere, which may also leave a signature in temperature, density or wind profiles. We have previously shown that variations in the eddy diffusion coefficient, can cause a wide range of significant correlated composition, thermal and wind changes.

REFERENCES

/1/ BARTH C.A., Reference Models for thermospheric NO., Adv. Space Res. (1989), (in press).

/2/ ROBLE R.G., E.C. RIDLEY and R.E. DICKINSON, On the global mean structure of the thermosphere, J. Geophys. Res., 92, 8745-87, (1987)

/3/ BANKS P.M. and G. KOCKARTS, Aeronomy, Parts A and B, Academic Press, New York, (1973).

/4/ Cospar Working Group IV, COSPAR International Reference Atmosphere (CIRA) 1972, Akademie-Verlag, Berlin, 1972.

/5/ HEDIN A.E., A revised thermospheric model based on mass spectrometer and incoherent scatter data: MSIS-83, J. Geophys. Res. 88, 10170, (1983).

/6/ HEDIN A.E., MSIS-86 thermospheric model, J. Geophys. Res. 92, 4649, (1987).

/7/ REES D., R. GORDON, T.J. FULLER-ROWELL, M.F. SMITH, G.R. CARIGNAN, T.L. KILLEEN, P.B. HAYS, N.W. SPENCER, The composition, structure, temperature and dynamics of the upper thermosphere in the polar regions during October to December 1981, Planet. Space. Sci. 33, 617, (1985).

/8/ REES D. and T.J. FULLER-ROWELL, Understanding the transport of atomic oxygen within the thermosphere, using a numerical global thermospheric model, Planet. Space Sci. 36, 935-948, (1988)

/9/ KOCKARTS, G., Nitric oxide cooling in the terrestrial thermosphere, Geophys. Res. Lett., 7, 137-140, (1980).

/10/ REES M.H., B.A. EMERY, R.G. ROBLE, and K. STAMNES, Neutral and ion gas heating by auroral electron precipitation, J. Geophys. Res., 88, 6289-6300, (1983).

/11/ RICHARDS P.G, M.R. TORR and D.G. TORR, Photo-dissociation of N_2, a significant source of thermospheric atomic nitrogen, J. Geophys. Res., 86, 1498-1498, (1981).

/12/ TORR M.R. and D.G. TORR, Chemistry of the thermosphere and ionosphere, J.Atm. Terr. Phys. 41, 797-839, (1979).

/13/ GARCIA R.R. and S. SOLOMON, J. Geophys Res 90, 3859, (1985)

/14/ FULLER-ROWELL T.J. and D. REES, A three-dimensional, time-dependent, global model of the thermosphere, J. Atmos. Sci., 37, 2545, (1980).

/15/ FULLER-ROWELL T.J. and D. REES, Derivation of a conservative equation for mean molecular weight for a two constituent gas within a three-dimensional, time-dependent model of the thermosphere, Planet. Space Sci., 31, 1209, (1983).

/16/ FULLER-ROWELL T.J., S. QUEGAN, D. REES, R.J. MOFFETT, G.J. BAILEY, Interactions between neutral thermospheric composition and the polar ionosphere using a coupled ionosphere-thermosphere model, J. Geophys. Res., 92, 7744, (1987).

/17/ FULLER-ROWELL T.J., Two-dimensional high resolution nested grid model of the thermosphere: 1 Neutral response to an electric field spike. J. Geophys. Res., 89, 2971-2990, (1984).

/18/ TORR M.R., D.E. TORR and R.A. ONG, Geophys. Res. Lett., 6, 771-774, (1979).

/19/ FULLER-ROWELL T.J. and D.S. EVANS, Height-integrated Pedersen and Hall conductivity patterns inferred from TIROS/NOAA satellite data. J. Geophys. Res. 92, 7606, (1987).

/20/ ROBLE R.G., and B.A. EMERY, On the global mean temperature of the thermosphere, Planet. Space Sci., 31, 597-614, (1983).

/21/ CHIU Y.T., An improved phenomenological model of ionospheric density, J. Atmos. Terr. Phys. 37, 1563-1570, (1975).

/22/ PARISH H., T.J. FULLER-ROWELL, D. REES, T.S VIRDI and P.J.S. WILLIAMS, Numerical simulations of the seasonal response of the thermosphere to propagating tides, Adv. Space Res., (1989), (in press)

/23/ MAYR H.G. and I. HARRIS, Some properties of upper atmosphere dynamics, Rev. Geophys and Space Phys., 16, 539, (1978).

AUTHOR INDEX